Control of the nematic-isotropic phase transition by an electric field

N. J. Mottram,[1,*] C. M. Care,[2] and D. J. Cleaver[2]
[1]*Department of Mathematics, University of Strathclyde, Glasgow G1 1XH, United Kingdom*
[2]*Materials and Engineering Research Institute, Sheffield Hallam University, Sheffield S1 1WB, United Kingdom*
(Received 10 November 2005; published 12 October 2006)

We use a relatively simple continuum model to investigate the effects of dielectric inhomogeneity within confined liquid-crystal cells. Specifically, we consider, in planar, cylindrical, and spherical geometries, the stability of a nematic-isotropic interface subject to an applied voltage when the nematic liquid crystal has a positive dielectric anisotropy. Depending on the magnitude of this voltage, the temperature, and the geometry of the cell, the nematic region may shrink until the material is completely isotropic within the cell, grow until the nematic phase fills the cell, or, in certain geometries, coexist with the isotropic phase. For planar geometry, no coexistence is found, but we are able to give analytical expressions for the critical voltage for an electric-field-induced phase transition as well as the critical wetting layer thickness for arbitrary applied voltage. In cells with cylindrical and spherical geometries, however, locally stable nematic-isotropic coexistence is predicted, the thickness of the nematic region being controllable by alteration of the applied voltage.

DOI: 10.1103/PhysRevE.74.041703 PACS number(s): 61.30.Hn, 61.30.Dk, 61.30.Gd

I. INTRODUCTION

The nematic-isotropic (*N-I*) phase transition is weakly first order, and so there exists a narrow temperature range over which the *N* and *I* phases coexist. In practice, however, for most systems the weakness of the *N-I* surface tension and the small enthalpy of the transition render experimental stabilization of *N-I* coexistence a considerable challenge. Thus, most direct observations of the *N-I* interface have relied on the imposition of a temperature gradient [1–3].

The conditions for *N-I* coexistence can also be influenced by the presence of disclinations, substrates, or impurities, since such inhomogeneities can seed regions of one symmetry at state points for which the other is stable in three-dimensional bulk. For example, order parameter variation at planar substrates has been observed in numerous experimental systems [4]. Indeed, there are a few cases where, by sandwiching a liquid crystal between substrates preferentially wet, respectively, by *N* and *I* phases and imposing precise temperature control, thermally equilibrated *N-I* interfaces have been obtained [5,6]. There are also numerous continuum and density functional treatments of liquid crystals adsorbed at substrates which show either partial or complete wetting by an *I* (*N*) film in the presence of a *N* (*I*) bulk [7,8]. Correspondingly, substrate-induced order parameter variation is a common finding in computer simulation studies of confined and adsorbed liquid crystals [9,10], leading to observation of phenomena such as capillary nematization and criticality of the bulk *N-I* transition [11,12].

A number of authors have also investigated the combined effects of applied bulk and surface fields on the *N-I* transition and wetting film growth [13,14] although few analytical results have been reported. An applied orienting field can influence both surface and bulk order and may induce a transition to the *N* phase even when the *I* phase is the global minimiser of the bulk thermotropic energy. In practice, however, orienting fields are not applied directly; rather, they develop due to voltages applied across the dielectric liquid crystal contained in the device. As such, spatial inhomogeneity in the electric field (reflecting any dielectric inhomogeneity) is perfectly possible and certainly must occur in situations involving, e.g., an isotropic liquid crystal confined between substrates which induce significant orientational order in the interfacial regions. This situation is complicated even further in cells with very-high-resolution electrode patterns, where these inhomogeneities are two dimensional [15].

In this paper we use a relatively simple continuum model to investigate the effect of dielectric inhomogeneity on the phase behavior of a liquid crystal subject to an applied voltage. In particular, we examine the possibility of using an applied voltage to control the relative thicknesses of *N* and *I* domains by exploiting the dielectric differences between the two phases. We note that there is an analogy [16] to be drawn here with the shear-induced banding induced in colloidal liquid-crystalline systems [17]. In these experiments, the system separates into *N* and *I* bands rather than adopting a continuous stress field across the entire shear cell [18]. Unlike these colloidal systems, however, the *N-I* interface in a single-component molecular system is characterized by a very small amplitude density step. Thus, unusually, the significant dielectric discontinuity seen at this interface has a very small associated compositional change. Consequently, formation of this particular phase boundary does not require substantial material transport.

The remainder of this paper is structured as follows. In the next two sections, we present the three geometries considered and detail, for each setup, the relevant contributions to the free energy of the system. In the subsequent section we give the resultant analysis for a planar-geometry cell. Following a description of the results obtained for this planar system, we then determine the corresponding results for systems with cylindrical and spherical geometries. Finally, the implications of these results are discussed.

II. GEOMETRIES

We consider liquid-crystal systems with three different geometries: planar, cylindrical, and spherical. In all three ge-

*Author to whom correspondence should be addressed. Electronic address: nigel.mottram@strath.ac.uk

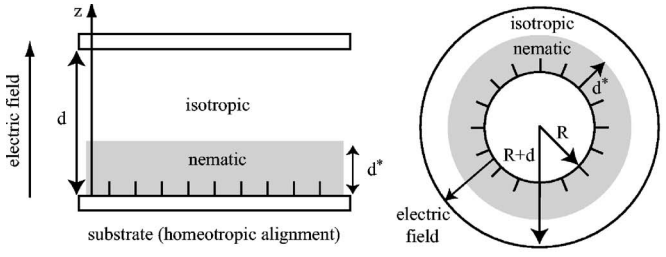

FIG. 1. Cell geometry: The liquid-crystalline material is sandwiched between two planar, cylindrical, or spherical substrates a distance d apart. The nematic layer, of thickness d^*, is taken to occur close to the homeotropically anchored substrate.

ometries we consider mesogenic material to be sandwiched between two substrates and hypothesize that, in the absence of an applied field, substrate-induced regions of N and I phases reside within this sandwich.

In the planar geometry the liquid-crystal material is sandwiched between two flat parallel substrates [see Fig. 1(a)], one of which favors homeotropic alignment. It is assumed that a region with N order is induced at one of the substrates due to partial or complete wetting [7]. As will be discussed later, it may not be necessary to assume such a layer preexists since an applied voltage may induce such a layer, although we will in general consider the evolution of such a layer of nematic as temperature and voltage are varied. It is further assumed that electrodes are deposited on the inner surfaces of the substrates so that an electric field may be applied in the direction parallel to the substrate normal, the z direction. The substrates are a distance d apart, and the N material occupies a region of thickness d^*, while the I phase fills the rest of the cell.

In the cylindrical and spherical geometries [see Figs. 1(b) and 1(c)] the liquid-crystal material fills the region between two concentric cylindrical or spherical shells, respectively. Here, electrodes are deposited on the inner face of the outer cylinder (sphere) and the outer face of the inner cylinder (sphere). Any applied electric field, therefore, points in the radial direction. The radii of the inner and outer cylinders (spheres) are R and $R+d$ and the nematic region, between $r=R$ and $r=R+d^*$, is taken to be adjacent to the inner cylinder (sphere).

III. FREE ENERGY

Our main concern in what follows is the effect of an applied voltage on the total thickness of the N region. Specifically, we consider whether the dielectric discontinuity associated with an N-I interface can be used to generate field-controllable domain thicknesses. To simplify the description of this system, we first assume that the nematic order parameter S is constant within each phase region and that the interfaces between the N and I regions have a finite and constant surface tension.

With the substrate adjacent to the N region inducing homeotropic alignment, the electric field assumed to be aligned with the z axis (in the planar case) or the local r axis (in the cylindrical and spherical cases), and the liquid crystal chosen to have a positive dielectric anisotropy, the director within the N layer can be taken to lie along the z axis (planar) or the radial direction (cylindrical, spherical). However, the electric field also induces an increase in order within both the N and I regions. In fact the I region becomes paranematic—that is, a state with nematic symmetry about the field axis but with a low order parameter. If we assume that the system remains uniaxial (a valid assumption since the homeotropically aligned surfaces do not induce biaxiality and, in this system, the dielectric effect of the field will tend to increase uniaxial order and reduce any biaxiality present), the liquid-crystalline order can be described by the symmetric traceless tensor

$$\mathbf{Q} = S(\mathbf{n} \otimes \mathbf{n} - \mathbf{I}/3), \tag{1}$$

where $\mathbf{I}$ is the identity tensor. The product $\mathbf{n} \otimes \mathbf{n}$ produces the 3×3 matrix with ijth entry equal to $n_i n_j$, the product of the ith and jth components of the director. The total free energy of the system, F, can then be expressed as the sum of a thermotropic energy contribution F_t, which describes the preference for the material to be in the N or I phase; an elastic distortion energy F_d; an electrostatic energy contribution F_e, which will be different in the paranematic and N regions due to the different permittivities of the phases; and an interfacial energy F_i for the N-I interface.

In the planar-geometry case there will be no distortion of the director and the interfacial area will be unchanged as the N region changes size. Therefore, in the planar case, the elastic contribution to the free energy will be zero and the interfacial contribution will be constant (with respect to changes in d^*).

In general, the free energy is

$$F = F_t + F_d + F_e + F_i = \int_{vol} (\mathcal{F}_t + \mathcal{F}_d + \mathcal{F}_e) \mathrm{d}v + \int_A \mathcal{F}_i \mathrm{d}s, \tag{2}$$

where, to recap, *vol* is the volume occupied by the combined N and I regions, A is the area of the N-I interface, and $\mathcal{F}$ denotes the appropriate free energy density contributions. Clearly, F is dependent on the order parameters within both the paranematic and N layers, S_I and S_N, respectively, and the total thickness of the N layer, d^*. Minimizing F with respect to these three variables, therefore, offers a route to determining the equilibrium states for these systems.

The minimization of the free energy can be performed using the standard equilibrium equations derived from the free energy:

$$\frac{\partial F}{\partial S_I} = 0, \quad \frac{\partial F}{\partial S_N} = 0, \quad \frac{\partial F}{\partial d^*} = 0. \tag{3}$$

However, in order to elucidate the behavior of a layer of nematic phase in the system as it evolves to its equilibrium

position we take a slightly different approach. The free energy depends on three variables: the order parameter in the paranematic layer, S_I; the order parameter in the nematic layer, S_N; and the thickness of the nematic layer, d^*. The energy surface $F(S_I,S_N,d^*)$ is hard to visualize graphically, and we will instead plot the free energy only as a function of d^* along the line of steepest descent. We do this by the following procedure. We first solve the S_I and S_N equilibrium equations simultaneously, either analytically in terms of d^* or numerically by specifying values of d^*. The solutions for S_I and S_N, in terms of d^*, are then used to find the energy of that state from the free energy expression. At this point we also check that the solution for S_I and S_N, for each value of d^*, is a local minimum of the energy by ensuring that the Hessian matrix

$$H = \begin{pmatrix} \frac{\partial^2 F}{\partial S_I^2} & \frac{\partial^2 F}{\partial S_N \partial S_I} \\ \frac{\partial^2 F}{\partial S_I \partial S_N} & \frac{\partial^2 F}{\partial S_N^2} \end{pmatrix} \tag{4}$$

is positive definite. In fact in all cases considered below the solutions of the equilibrium equations (3a) and (3b) lead to minima with respect to S_I and S_N. Therefore, a minimum with respect to d^* will correspond to a local minimum in the free energy while a maximum with respect to d^* will correspond to a saddle point.

This approach then gives us the free energy in terms of d^*, either analytically or as a set of numerical free energy values for the set of numerical values of d^*. This enables us to plot $F(d^*)$, and since for each value d^* this is the local minimum energy with respect to S_I and S_N, it indicates the line of steepest descent on the free energy surface $F(S_I,S_N,d^*)$ projected onto the F-d^* plane. We can therefore be sure that any minimum in the $F(d^*)$ plot will represent a local minimum of the free energy. It is impossible to state that this is the global minimizer of the free energy since there will be many possible configurations of the system (e.g., multiple N/I layers within the region of different order parameters) but we can check that any such minimum in $F(d^*)$ has an energy lower than obvious alternative possibilities such as a completely isotropic region of a completely nematic region. These plots of $F(d^*)$ will then enable us to gain a qualitative insight into how the system will attempt to attain its minimum energy by altering the nematic layer thickness d^*.

It should also be mentioned that in this work we have assumed that no substrate energy terms enter the free energy expression. This is a simplification of the model, and a fuller model would include such terms. However, such an addition will not change the results qualitatively, and as we will discuss later, in some cases, the presence of a substrate which favors the nematic phase is not necessary to induce a nematic layer.

A. Thermotropic energy

Following the classic Landau–de Gennes treatment [13], the thermotropic energy density of the nematic is approximated using a truncated Taylor expansion in the tensor order parameter,

$$\mathcal{F}_t = \mathcal{F}_0 + \frac{a}{2}\mathrm{tr}(\mathbf{Q}^2) + \frac{b}{3}\mathrm{tr}(\mathbf{Q}^3) + \frac{c}{4}[\mathrm{tr}(\mathbf{Q}^2)]^2, \tag{5}$$

where $\mathcal{F}_0$ is the energy density of the I phase and tr denotes the trace operator. In principle, the coefficients a, b, and c can all be temperature dependent, although it is usual to assume that $a=\alpha(T-T^*)$ is linear in temperature T, while α, b, and c are all constants. In this expression, T^* is the supercooling limit, the temperature at which the I phase becomes unstable.

Using the uniaxial expression for $\mathbf{Q}$ given in Eq. (1) the thermotropic energy then becomes

$$\mathcal{F}_t = \mathcal{F}_0 + \frac{\alpha}{3}(T-T^*)S^2 + \frac{2b}{27}S^3 + \frac{c}{9}S^4 = \mathcal{F}_0 + \sigma(S), \tag{6}$$

where the shorthand notation $\sigma(S)$ will be used in later sections. The constant $\mathcal{F}_0$ will not enter the energy minimization and will therefore be neglected in future expressions. There are, at most, three extrema of this thermotropic energy expression, the I phase $S=0$ and two N states $S_+=[-b+\sqrt{b^2-24\alpha c(T-T^*)}]/4c$ and $S_-=[-b-\sqrt{b^2-24\alpha c(T-T^*)}]/4c$ (one at least locally stable and one unstable). There are also three significant temperatures: the temperature at which the I phase ceases to be metastable, the supercooling limit T^*; the temperature at which the energy density of the I phase $S=0$ and the energy density of the N phase $S=S_+$ are equal, the clearing point, given by $T_{NI}=T^*+b^2/27ac$; and the temperature above which the N phase ceases to be metastable, the superheating limit given by $T^+=T^*+b^2/24ac$. Within the temperature range $T<T^+$ the state $S=S_+$ is the relevant (at least locally) stable N state. With parameter values $\alpha=1.5\times10^5$ J m^{-3} K^{-1}, $b=-2.25\times10^6$ J m^{-3}, and $c=4.5\times10^6$ J m^{-3} the superheating and clearing points are $T^+=T^*+0.3125$ K and $T_{NI}=T^*+0.2778$ K. The values for α, b, and c used here are generic values of the same order of magnitude as the relatively few sets of data found in the literature (e.g., [19]). Altering these values to those measured for a specific material would not change the subsequent results qualitatively.

B. Electrostatic energy

Assuming an absence of permanent dipoles or free charges, the electrostatic energy within a dielectric material is the sum of the background electrostatic energy which would be present in vacuum and the extra energy derived from the dipoles which are induced when a voltage is applied across the cell. The electrostatic free energy is therefore a function of the permittivity of the dielectric material and is expressed by

$$\mathcal{F}_e = -\int \mathbf{D}\cdot d\mathbf{E} = -\frac{1}{2}\epsilon_0(\boldsymbol{\epsilon}\cdot\mathbf{E})\cdot\mathbf{E}, \tag{7}$$

where $\mathbf{E}$ is the electric field, $\mathbf{D}=\epsilon_0\boldsymbol{\epsilon}\mathbf{E}$ is the displacement field, ϵ_0 is the permittivity of free space, and $\boldsymbol{\epsilon}$ is the dielectric permittivity tensor.

Using Maxwell's equations, in the planar, cylindrical, and spherical cases, for a charge-free system it is then relatively

straightforward to show that the electric field in the substrate normal direction is

$$E_z(z) = \frac{1}{\epsilon_0 \epsilon_{zz}(z)} \left(\frac{-V}{\int_0^d \frac{1}{\epsilon_0 \epsilon_{zz}(z)} \mathrm{d}z} \right) \tag{8}$$

for the planar case,

$$E_r(r) = \frac{1}{\epsilon_0 \epsilon_{rr}(r)} \frac{1}{r} \left(\frac{-V}{\int_R^{R+d} \frac{1}{\epsilon_0 \epsilon_{rr}(r)} \frac{1}{r} \mathrm{d}r} \right) \tag{9}$$

for the cylindrical case, and

$$E_r(r) = \frac{1}{\epsilon_0 \epsilon_{rr}(r)} \frac{1}{r^2} \left(\frac{-V}{\int_R^{R+d} \frac{1}{\epsilon_0 \epsilon_{rr}(r)} \frac{1}{r^2} \mathrm{d}r} \right) \tag{10}$$

for the spherical case. Here V is the potential difference between the two substrates (with the higher voltage applied at the upper and outer surfaces) and $\epsilon_{zz}(z)$ and $\epsilon_{rr}(r)$ are the zz and rr components of the dielectric tensor which may change through the cell.

Writing the dielectric tensor as [19]

$$\boldsymbol{\epsilon} = \bar{\epsilon}\mathbf{I} + \Delta\epsilon^* \mathbf{Q}, \tag{11}$$

and assuming uniaxiality throughout the cell, Eq. (1) with $\mathbf{n}=\mathbf{e}_z$ or $\mathbf{n}=\mathbf{e}_r$, depending on the geometry, then leads to

$$\epsilon_{zz} \quad \text{or} \quad \epsilon_{rr} = \bar{\epsilon} + \frac{2\Delta\epsilon^* S}{3}, \tag{12}$$

where $\bar{\epsilon}=(\epsilon_\parallel+2\epsilon_\perp)/3$ is the permittivity of the I phase and $\Delta\epsilon^*=(\epsilon_\parallel-\epsilon_\perp)/S_{expt}$ is the dielectric anisotropy, which is assumed to be positive, scaled by the order parameter at which the experimentally determined permittivity values were taken, S_{expt}. Denoting the order parameter in the N phase as S_N and that in the I/paranematic phase as S_I then gives, in the respective phase regions, $\epsilon_N=\bar{\epsilon}+2\Delta\epsilon^* S_N/3$ and $\epsilon_I=\bar{\epsilon}+2\Delta\epsilon^* S_I/3$.

In the three geometries we consider here, there are N and paranematic regions, with fixed permittivity tensors $\boldsymbol{\epsilon}_N$ and $\boldsymbol{\epsilon}_I$, respectively. Because of the simplicity of the geometries considered, the free energy densities, Eq. (7), may then be written as

$$\mathcal{F}_e = -\frac{1}{2}\epsilon_0 \epsilon_{zz} E_z^{\,2} \quad \text{or} \quad -\frac{1}{2}\epsilon_0 \epsilon_{rr} E_r^{\,2} \tag{13}$$

for the planar and nonplanar geometries, respectively. The forms of E_z, E_r, ϵ_{zz}, and ϵ_{rr} are then given by Eqs. (8)–(10) and Eq. (12) so that the integrals needed to calculate the electrostatic energy in the different regions can be evaluated analytically.

C. Elastic energy

The elastic energy of the material is defined in both the N and paranematic region but a true I phase will not support equilibrium elastic distortion. We use the standard expression for elastic energy as a function of the $\mathbf{Q}$ tensor for an achiral nematic material [19]:

$$F_d = \frac{L_{11}}{2}\frac{\partial Q_{ij}}{\partial x_k}\frac{\partial Q_{ij}}{\partial x_k} + \frac{L_{22}}{2}\frac{\partial Q_{ij}}{\partial x_j}\frac{\partial Q_{ik}}{\partial x_k} + \frac{L_{33}}{2}\frac{\partial Q_{ik}}{\partial x_j}\frac{\partial Q_{ij}}{\partial x_k}, \tag{14}$$

where the L_{ii} are elastic constants and summation over repeated indices is assumed. This relatively simple expression assumes that the splay and bend elastic constants (the Frank constants K_{11} and K_{33}) of the liquid crystal are equal. Higher-order terms could be used to distinguish between these elastic distortions but in our system only splay distortions will be present and therefore only the constant L_{11} occurs in the free energy.

For the planar case, when $\mathbf{n}=\mathbf{e}_z$ there is no distortion and the elastic-energy density is zero. However, for the cylindrical and spherical cases the director exhibits a splayed structure $\mathbf{n}=\mathbf{e}_r$ and the elastic energy density, Eq. (14), becomes

$$\mathcal{F}_d = \frac{L_{11}S^2}{2}\frac{1}{r^2} \tag{15}$$

and

$$\mathcal{F}_d = 2L_{11}S^2\frac{1}{r^2}, \tag{16}$$

respectively. The elastic energy, in the cylindrical and spherical geometries, can therefore be calculated by integrating Eq. (15) or (16), respectively, over the nematic (where $S=S_N$) and paranematic (where $S=S_I$) regions.

D. Interfacial energy

The interfacial energy density can be approximated if we consider a phase boundary profile of the form [20]

$$S = \frac{S_N + S_I}{2} + \frac{S_N - S_I}{2}\tanh\left(\frac{x}{w}\right), \tag{17}$$

where w is the width of the phase boundary and the distortion energy density of the form $(\boldsymbol{\nabla} S)^2$. The interfacial energy density is then proportional to the square of the difference between the order parameters in the N and paranematic regions,

$$\mathcal{F}_i = \gamma(S_N - S_I)^2, \tag{18}$$

and therefore the interfacial energy is simply

$$F_i = \gamma A(S_N - S_I)^2, \tag{19}$$

where A is the area of the interface and γ is a surface tension parameter for the N-paranematic interface. In the planar geometry the interfacial area is simply $A=l_x l_y$, the area of the cell. In the cylindrical case $A=2\pi(R+d^*)l_z$ where l_z is the extent of the cylinder in the z direction. In the spherical case the interface area is $A=4\pi(R+d^*)^2$.

For each of the geometries considered below we have also calculated the free energy of a completely isotropic or a completely nematic layer in order to compare to states which include an interface. For the completely isotropic or nematic states the interfacial energy is ignored.

IV. PLANAR GEOMETRY

In the planar geometry shown in Fig. 1(a) the electric field expression in Eq. (8) may be evaluated analytically by setting $\epsilon_{zz}=\epsilon_N$ in $0<z<d^*$ and $\epsilon_{zz}=\epsilon_I$ in $d^*<z<d$. The electric fields within the N and I regions then become

$$\mathcal{F}_e^N = -\frac{\epsilon_0\epsilon_I}{2}\frac{V^2\epsilon_I\epsilon_N}{[d^*(\epsilon_I-\epsilon_N)+d\epsilon_N]^2},$$

$$\mathcal{F}_e^I = -\frac{\epsilon_0\epsilon_N}{2}\frac{V^2\epsilon_I\epsilon_N}{[d^*(\epsilon_I-\epsilon_N)+d\epsilon_N]^2}. \tag{20}$$

Splitting the free energy in Eq. (2) into the N and I regions and using the free energy densities in Eqs. (6), (20), and (18) then gives

$$F = l_x l_y\left(\int_0^{d^*}\sigma(S_N) - \frac{\epsilon_0\epsilon_I}{2}\frac{V^2\epsilon_I\epsilon_N}{[d^*(\epsilon_I-\epsilon_N)+d\epsilon_N]^2}\mathrm{d}z + \int_{d^*}^{d}\sigma(S_I) - \frac{\epsilon_0\epsilon_N}{2}\frac{V^2\epsilon_I\epsilon_N}{[d^*(\epsilon_I-\epsilon_N)+d\epsilon_N]^2}\mathrm{d}z + \gamma(S_N-S_I)^2\right), \tag{21}$$

where l_x and l_y are the extents of cell in the x and y directions. Upon integration, Eq. (21) leads to

$$F/(l_x l_y) = [d^*(\sigma(S_N)-\sigma(S_I))+d\sigma(S_I)] - \frac{1}{2}\frac{\epsilon_0\epsilon_I\epsilon_N V^2}{d^*(\epsilon_I-\epsilon_N)+d\epsilon_N} + \gamma(S_N-S_I)^2. \tag{22}$$

This energy has a singularity at $d^*=d\epsilon_N/(\epsilon_N-\epsilon_I)$, but since it has been assumed that the material has a positive dielectric anisotropy, we have $0<\epsilon_I<\epsilon_N$ so that the singularity occurs for the nonphysical region $d^*>d$. With the applied voltage set to zero, this free energy is linear in d^* and thus minimization with respect to d^* leads to the results $d^*=0$ (i.e., no N region) if $\sigma(S_N)>\sigma(S_I)$ and $d^*=d$ (i.e., a fully N cell) if $\sigma(S_N)<\sigma(S_I)$. In this case, where $V=0$, minimization of the free energy with respect to S_I and S_N can also be carried out. When $\gamma=0$ the solutions are simply $S_I=0$ and $S_N=S_+$. With a realistic value, $\gamma=1.0\times10^{-5}$ N m^{-1}, these solution change very little since the effect of the interfacial energy is small compared to the thermotropic energy [because $\gamma\ll d\alpha\Delta(T-T^*)$].

When a voltage is applied to the cell, however, the minimization becomes more complicated due to the dependence of ϵ_I and ϵ_N on S_I and S_N. Very little analytical progress can be made with the full description of this situation, and the free energy must be minimized numerically (see below). However, if we assume that the applied voltage does not significantly alter the order parameter in either region, then an approximate analytical solution *may* be found. Assuming that the dielectric contribution to the energy is small compared to the thermotropic contribution is equivalent to having

$$\frac{\epsilon_0\bar{\epsilon}V^2}{d} \ll d\beta, \tag{23}$$

where β is of the same order as the thermotropic Landau–de Gennes coefficients a, b, and c. Since $\epsilon_0=8.854\times10^{-12}$ F m^{-1} and, typically, $d\sim10^{-5}$ m, $\beta\sim10^6$ J m^{-3}, and $\bar{\epsilon}\sim10^1$, this is equivalent to $V\ll10^3$ V which is well above the voltages applied in typical devices. We can, therefore, be relatively confident in using $(\epsilon_0\bar{\epsilon}V^2)/(d^2\beta)=\delta$ as a small parameter. A perturbation analysis can then be carried out using the assumption that, when $\delta\ll1$, the N and paranematic order parameters can be approximated by expansion series about the values $S_N=S_+$ and $S_I=0$,

$$S_N = S_+ + \delta S_{N1} + O(\delta^2), \tag{24}$$

$$S_I = \delta S_{I1} + O(\delta^2). \tag{25}$$

Solutions for S_{N1} and S_{I1}, as well as higher-order terms in the expansions, can readily be found analytically, although these expressions are lengthy and are not presented here. Using the resulting approximations from Eqs. (24) and (25), substituted into the total energy, we then obtain the free energy as a function of d^* only which is, as explained above, the line of steepest descent on the energy surface $F(S_I,S_N,d^*)$, projected onto the F-d^* plane.

To illustrate the predictions of this approach, we show, in Fig. 2, plots of the free energy as a function of domain size d^* for various voltages but for a fixed temperature $T=T^*+0.28$ K, which is between $T^+=T^*+0.3125$ K and $T_{NI}=T^*+0.2778$ K, so that the N phase is metastable. Other parameter values are $\alpha=1.5\times10^5$ J m^{-3} K^{-1}, $b=-2.25\times10^6$ J m^{-3}, $c=4.5\times10^6$ J m^{-3}, $\epsilon_\perp=4.2$, $\epsilon_\parallel=9.6$, $S_{expt}=0.6$ (so that $\Delta\epsilon^*=9$ and $\bar{\epsilon}=6$), $\epsilon_0=8.854\times10^{-12}$ F m^{-1}, $\gamma=1.0\times10^{-5}$ N m^{-1}, and $d=1.0\times10^{-5}$ m. The shaded area, where $d^*<0$ or $d^*>d$, is outside the range of physically achievable domain sizes and so can be disregarded.

Figure 2 shows the energy plot resulting from a numerical minimization of the full free energy expression (22) with respect to S_I and S_N (which, as described above, only ensures that there exists a local minimum), as well as the analytical results obtained using both the perturbation solution [based on the expansions (24) and (25)] and the most basic free energy expression which assumes $S_I=0$ and $S_N=S_+$. We note that it is not possible to differentiate between these three sets of plots, the percentage difference between the numerical solution and the approximate solutions being at most 0.05%. This means that not only is the perturbation expansion solution an excellent approximation to the numerical solution, but even the crude simplification $S_I=0$, $S_N=S_+$ is also extremely accurate.

With the simplification $S_I=0$, $S_N=S_+$ we may go further analytically. By differentiating the free energy equation (22) with respect to d^* we find that there are stationary points of the energy at

$$d^*_{max} = \frac{d\epsilon_N}{(\epsilon_N-\epsilon_I)} - |V|\sqrt{\frac{\epsilon_0\epsilon_N\epsilon_I}{2(\epsilon_N-\epsilon_I)\sigma(S_+)}}, \tag{26}$$

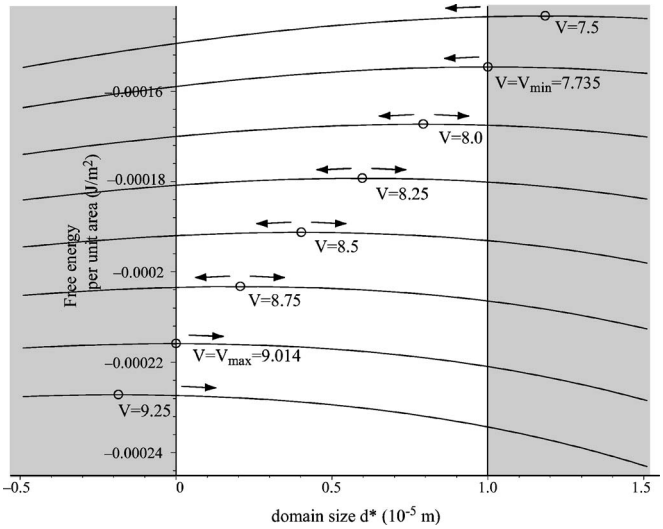

FIG. 2. Planar geometry: the total free energy as a function of domain size d^* for voltages $V=7.5$ V, $V_{min}=7.735$, 8.0, 8.25, 8.5, 8.75 V, and $V_{max}=9.014$ and 9.25 V. As indicated by the arrows, for domain sizes less than the critical size (denoted by a circle for each voltage) where the maximum energy occurs, the system energy is reduced by shrinking the domain size to zero. For domains of size greater than the critical size, the system energy is reduced by growing the domain size to fill the cell. Three plots are shown for each parameter set (numerical solution of full problem and two analytical solutions to perturbation expansions—see text for details) but they cannot be resolved on the scale of this figure.

$$d^*_{min} = \frac{d\epsilon_N}{(\epsilon_N - \epsilon_I)} + |V| \sqrt{\frac{\epsilon_0 \epsilon_N \epsilon_I}{2(\epsilon_N - \epsilon_I)\sigma(S_+)}}, \tag{27}$$

where, as indicated by the subscripts, it is possible to show [by considering $d^2\bar{F}/d(d^*)^2$] that d^*_{max} is a maximum (with respect to variations in d^*) of the energy and d^*_{min} is a minimum (with respect to variations in d^*) of the energy. As mentioned above, the maximum with respect to d^* corresponds to a saddle point of the free energy. However, these maximum and minimum points only exist when $\sigma(S_+)>0$—that is, when $T>T_{NI}$. For physical significance, it is also necessary for the nematic phase to exist at least as a metastable state and, therefore, we must also have $T<T^+$. From Eqs. (26) and (27) we can also see that, since $\epsilon_N>\epsilon_I$, we obtain $d^*_{min}>d$ and, thus, the locally stable equilibrium case is never physically relevant for this system geometry. The value of d^* corresponding to an energy maximum, given by Eq. (26), *is* physically relevant in some cases; these values are indicated by the open circles in Fig. 2. From these, we see that, for cases with a total N domain width smaller than d^*_{max}, the N domains will shrink to leave the cell filled with the I fluid whereas when the total N domain width is larger than d^*_{max} the N domain will grow and fill the cell.

The maximum point lies within the cell—that is, $0<d^*<d$—when

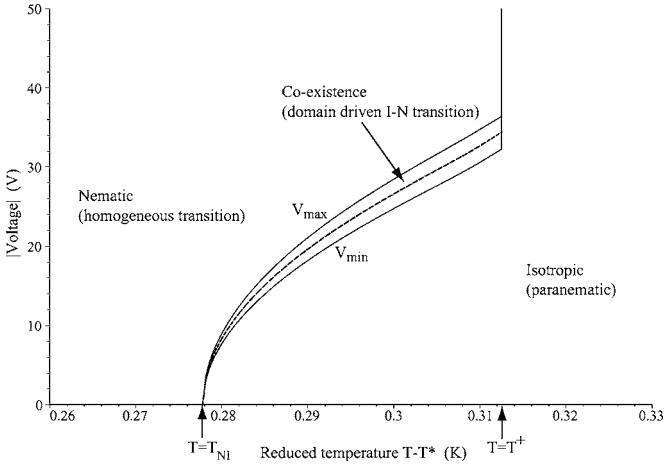

FIG. 3. The voltage-temperature phase diagram for the planar geometry: there exists a region, between the curves V_{min} and V_{max}, where the stable state can be either fully nematic or fully isotropic, depending on the width of the nematic domain present in the system. The critical size of the domain necessary to induce the domain-induced transition to a fully nematic cell depends on both T and V. For instance, along the dashed line a nematic domain thickness corresponding to half of the cell width is necessary to induce a fully nematic state.

$$V_{min} = d\sqrt{\frac{2\epsilon_I \sigma(S_+)}{\epsilon_0 \epsilon_N (\epsilon_N - \epsilon_I)}} < V < d\sqrt{\frac{2\epsilon_N \sigma(S_+)}{\epsilon_0 \epsilon_I (\epsilon_N - \epsilon_I)}} = V_{max}. \tag{28}$$

Therefore, for any fixed temperature between T_{NI} and T^+, there exists a minimum voltage such that for $V<V_{min}$, even a substrate-induced domain of size $d^*=d$ (the full cell filled with N) will not be able to maintain the cell in the N phase. The energy curve in Fig. 2 with $V=7.5$ V is such a situation where an N domain of any size will shrink to leave an I cell. There is also a corresponding maximum voltage V_{max} above which a surface domain of size $d^*=0$ will be unstable with respect to the full phase transition of the cell from I to N. In such cases, N order will develop at all points in the cell and, therefore, the transition from N to I will be homogeneous and not domain driven. In other words, any applied voltage $V>V_{max}$ will lead to a homogeneous I-N transition.

The behavior of this field-induced seeding is summarized in the phase diagram in Fig. 3. For temperatures between T_{NI} and T^+ no field-induced I-N transition is possible for voltages $V<V_{min}$. At fixed T in this temperature range, however, a field-induced transition to the N phase, through domain growth, will be possible for voltages in the range $V_{min}<V<V_{max}$. The precise value of V needed to induce this domain-growth process will depend on the inherent domain size in the system. Thus, for substrates which are completely wetted by a N film (leading to large d^*), a voltage close to V_{min} will suffice, whereas partially wet substrates will require $V \lesssim V_{max}$. This raises an intriguing prospect for patterned surfaces, that this domain growth will directly project the degree of surface-induced order into the state adopted across the entire cell width. For applied voltages greater than $V_{max}(T)$ a homogeneous transition occurs in this temperature

region. For temperatures greater than T^+ the N phase is not a stable state and, therefore, the field-induced transition is not possible, although the orienting effect of the applied field will induce some paranematic order within the fluid.

V. NONPLANAR GEOMETRIES

In the analysis presented in the previous section, the substrates confining the liquid crystal were taken to be planar and parallel. In this geometry, it was found that the global minimum of the free energy always corresponds to either a fully N or a fully I cell. For certain narrow ranges of voltage and temperature, however, the state adopted by the system was found to be controlled, in part, by the extent of any substrate-induced ordered domain. Indeed, for temperatures between T_{NI} and T^+, it was shown that discontinuous switching from fully N to fully I states could be induced by simply changing the applied voltage (see Fig. 3) but no locally stable equilibrium states were found involving an N-I interface.

As we shall now show, however, equivalent analysis performed for cells with a nonplanar geometry *does* predict arrangements corresponding to field-stabilized N-I coexistence over the limited temperature range $T_{NI} \leqslant T \leqslant T^+$. Specifically, we show that for cylindrical and spherical cells it is possible to find a range of cell dimensions and voltages for which the global free energy is minimized (at least locally) by a state which includes a N-I interface. This effect occurs because, in these geometries, the electric field cannot be uniform throughout space; hence, in some situations, the global free energy may be minimized if the region of the cell with the stronger electric field is N while the remainder of the cell remains I.

In a nonplanar geometry there is a nonzero contribution to the free energy from distortions in the director field and the free energy of the N-I interface is also dependent upon the position of the interface. Despite these additional effects and subject to the assumption that it is valid to ignore any change in the order parameter due to the splay deformation, it is found that for typical values of the material parameters, a field-banded arrangement with a N-I interface can be the locally stable state.

A. Cylindrical case

If we consider a system with cylindrical geometry, with an inner cylinder of radius R and a concentric outer cylinder of radius $R+d$ [see Fig. 1(b)], we may follow similar arguments to those in the previous section to show that the contributions to the free energy contributions are given by

$$F_t/l_z = \pi[\sigma(S_I)(d-d^*)(d+d^*+2R) + \sigma(S_N)d^*(d^*+2R)],$$

$$F_e/l_z = \frac{\pi V^2 \varepsilon_0 \varepsilon_N \varepsilon_I}{\varepsilon_I[\ln(R) - \ln(d^*+R)] + \varepsilon_N[\ln(d^*+R) - \ln(d+R)]},$$

$$F_d/l_z = \pi L_{11}[S_I^2\{\ln(d+R) - \ln(d^*+R)\} + S_N^2\{\ln(d^*+R) - \ln(R)\}],$$

$$F_i/l_z = 2\pi\gamma(d^*+R)(S_I - S_N)^2, \tag{29}$$

where l_z is the extent of the cylinder in the z direction. Note, for consistency with the results presented in Sec. IV, that in the limit of large radius, the above expressions for F_t, F_e, and F_i, scaled by the surface area of the inner sphere, asymptote to the corresponding terms in the equivalent planar geometry expression [Eq. (22)]. In the limit of large radius the expression for the elastic energy F_d tends to zero, as expected for the planar case.

However, it is not possible to progress analytically with this set of equations. Resorting to numerical calculations, therefore, we plot, in Fig. 4, the free energy of this system per unit length in the z direction. Here, we have used the same temperature, cell thickness, and material parameter values as those employed in our planar-geometry calculations with, additionally, $\gamma = 1.0 \times 10^{-5}$ N m^{-1} and $L_{11} = 1.0 \times 10^{-11}$ N which are typical values for the surface tension [2] and elastic constants [19]. As before, in the planar case, the construction of Fig. 4 is essentially the same. From the free energy in Eq. (29) we find the equilibrium equations for S_I and S_N and by specifying a numerical value of d^* and numerically solving these equations we find the energy of that state from Eq. (29). We continue this process for a range of d^* and R values, creating the plot in Fig. 4.

These results show that for a large inner cylinder radius the behavior is similar to that found for the planar case [Fig. 4(a)]: a nematic region will either expand to fill the region if d^* is greater than some critical value or the I layer will expand to fill the region if d^* is smaller than the critical value. However, when the radius R of the inner sphere is reduced, a significant range of applied voltages exists for which the free energy has a *local minimum* for $0 < d^* < d$; i.e., there is a locally stable N-I interface between the inner and outer cylinders [Fig. 4(b)]. Furthermore, other sets of results (not shown here) indicate that if the radius of the outer conductor and the applied voltage are increased sufficiently, it is possible to achieve thick N layers. It must be emphasized, however, that such coexistence only occurs over the narrow temperature range for which both the N and I phases are either stable or metastable.

B. Spherical case

If we now consider a system with spherical symmetry consisting of an inner conductor of radius R surrounded by a concentric outer sphere of radius $R+d$ [Fig. 1(c)], the free energy contributions can be expressed as

$$F_t = \frac{4}{3}\pi\{\sigma(S_I)[(R+d)^3 - (R+d^*)^3] + \sigma(S_N)[(R+d^*)^3 - R^3]\},$$

$$F_e = -\frac{2\pi\varepsilon_0\varepsilon_N\varepsilon_I R(d+R)(d^*+R)V^2}{\varepsilon_I d^*(d+R) + \varepsilon_N R(d-d^*)},$$

$$F_d = 8\pi L_{11} d^* S_N^2,$$

$$F_i = 4\pi\gamma(d^*+R)^2(S_I - S_N)^2. \tag{30}$$

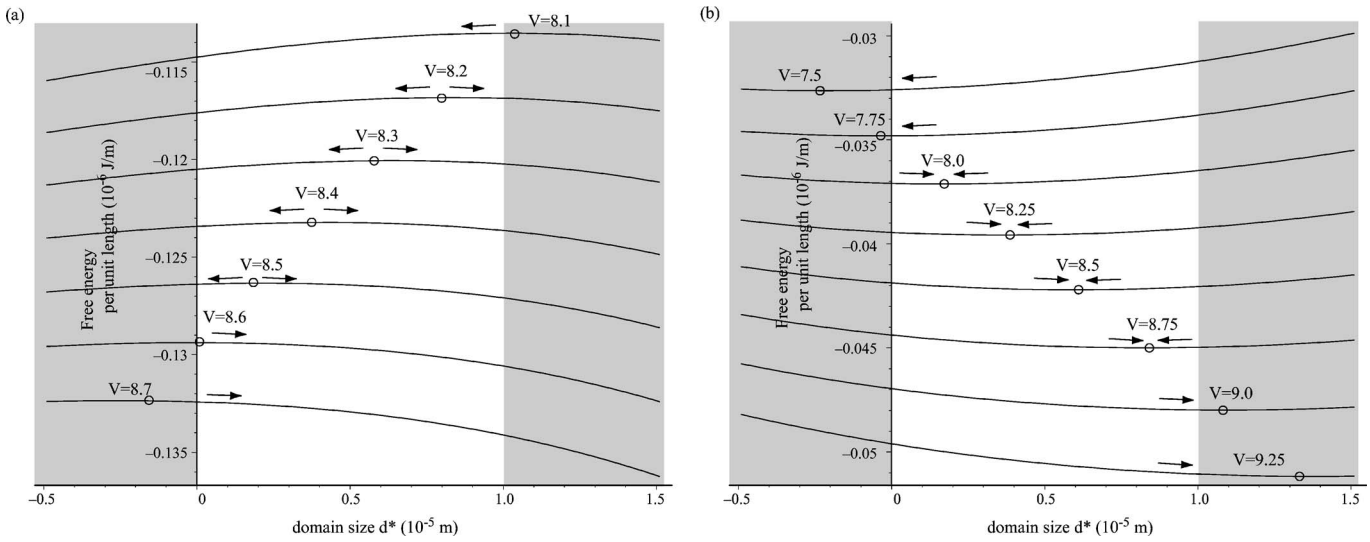

FIG. 4. Cylindrical geometry: the total free energy as a function of domain size d^* for (a) inner cylinder radius $R=10\times10^{-5}$ m and voltages $V=8$, 8.25, 8.5, 8.75 V and (b) inner cylinder radius $R=3\times10^{-5}$ m and voltages $V=7.5$, 7.75, 8, 8.25, 8.5, 8.75, 9, 9.25 V. At small R, the free energy has a minimum within the cell, implying a coexistence or banding of the nematic and isotropic phases.

It is again not possible to progress analytically with this set of equations. However, as in the cylindrical case, we may plot the total energy as a function of d^* by evaluating S_I and S_N in Eqs. (30) by numerical minimization. We may also use the simple assumption that $S_I=0$ and $S_N=S_+$ to simplify the total energy; as shown above, this is an extremely good approximation to the full energy expression.

Using the same parameter values as those employed in the cylindrical case, we show, in Figs. 5(a) and 5(b), energy plots for a range of voltages and for $R=50\times10^{-5}$ m and $R=5\times10^{-5}$ m, respectively. As in the cylindrical case, when the radius R of the inner sphere is reduced sufficiently, there is a significant range of applied voltages for which a locally stable N-I interface develops between the inner and outer spheres.

VI. CONCLUSIONS

Using a relatively simple model of the effect of an applied voltage on the I to N phase transition, we have investigated the stability of the N-I interface under the influence of various electric field patterns. In the case of a planar geometry system, we have found that the N-I interface cannot be stabilized by the effects of dielectric inhomogeneity alone. Here, though, we have been able to find analytic expressions for the critical domain size, Eq. (26), and critical voltage, Eq. (28), at which field-induced transitions occur. Thus, from Eq. (26), we see that the critical domain size d^*_{max} is linearly proportional to the modulus of the applied voltage and its temperature dependence is of the form $-(T-T_{NI})^{-1/2}$ due to the temperature dependence of $\sigma(S_+)$. Therefore, as the tem-

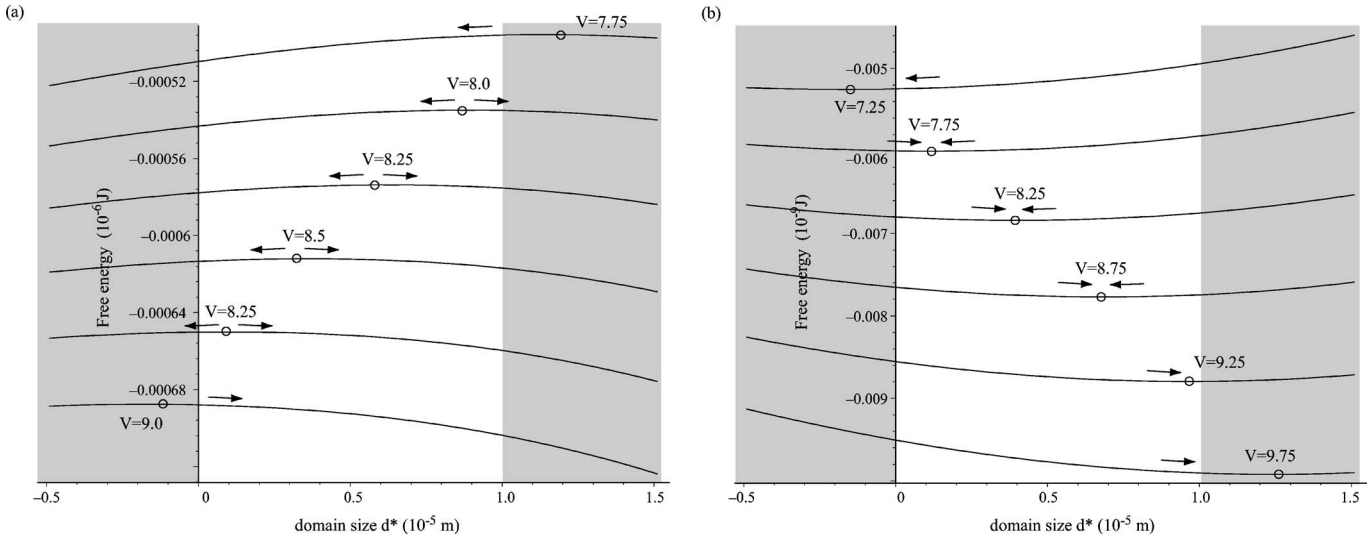

FIG. 5. Spherical geometry: the total free energy as a function of domain size d^* for (a) inner sphere radius $R=50\times10^{-5}$ m and voltages $V=7.75$, 8, 8.25, 8.5, 8.75, 9 V and (b) inner sphere radius $R=5\times10^{-5}$ m and voltages $V=7.25$, 7.75, 8.25, 8.75, 9.25, 9.75 V. At small R, the free energy has a minimum within the cell, implying a coexistence or banding of the nematic and isotropic phases.

perature decreases towards T_{NI} the critical domain size decreases, eventually leading to a homogeneous transition where domains are not necessary to seed the transition. From the minimum and maximum critical voltages in Eq. (28) we find that $V_{min}/V_{max}=\epsilon_I/\epsilon_N$ so that for a weakly anisotropic materials, where $\epsilon_N \approx \epsilon_I$, the range of voltages which induce a domain-driven phase transition will be small.

For the cylindrical and spherical geometries we have found that it *is* possible, for a range of cell dimensions and voltages, to generate a locally stable *N-I* interface in the interior of the liquid-crystal region. Furthermore, we have shown that, by changing the applied voltage, the interface position can be controlled and so moved to any point in the cell. The free energy versus interface position plots show that a cell with $d^*=d$ or a cell with $d^*=0$ may not be the lowest-energy state and that a banded nematic/paranematic cell is preferred. These two possibilities $(d^*=d, d^*=0)$ do not quite represent cells which are completely filled with nematic and paranematic, respectively, because of the inclusion of the interface energy (which remains even if $d^*=d$ or $d^*=0$). However, even when we neglect this energy term in order to compare a banded cell with a fully nematic or fully isotropic cell, we find that the banded cell is still of lower energy for a range of voltages. Therefore a nematic layer should spontaneously grow from the inner substrate even if there is no preference for that substrate to induce nematic order.

One limiting factor in drawing such conclusions is that this effect may be restricted to a small temperature range around T_{NI}. Other influences such as impurities in the nematic liquid crystal, surface inhomogeneities, and thermal fluctuations may also play a role in destabilizing the nematic and paranematic coexistence. Such effects are hard to quantify, and experimental measurement is clearly needed to confirm these results.

This result suggests a generally applicable route to stabilizing *N-I* interfaces which has no recourse to, e.g., material-specific surface treatments. Such direct access to the *N-I* interface should enable assessment of the various molecular theories relating to this area. Furthermore, there is interest in being able to continuously vary liquid-crystal film thicknesses in the submicron range. This is particularly of interest in hybrid aligned nematic films where elastic theory predicts qualitative changes in the **Q**-tensor profile as the film thickness is reduced [21] but experiment and simulation suggest structural effects neglected by continuum methods [22,23].

Our findings may also have some technological application. Most obviously, our predictions for the cylindrical geometry lead directly to the concept of active optical fibers in which the radius of the refractive index step can be varied in time and/or distance along the fiber. As noted above, for single-component molecular mesogens, this controllable dielectric interface has little associated compositional change, making material transport a secondary consideration. Alternatively, liquid-crystal mixtures or even polymeric-mesogen systems could be used, so as to increase the available thermal range of *N-I* coexistence at the cost of significantly slower switching times.

ACKNOWLEDGMENT

N.J.M would like to thank the EPSRC for funding.

[1] D. Langevin-Cruchon and M. A. Bouchiat, Mol. Cryst. Liq. Cryst. **22**, 317 (1973).
[2] S. Faetti and V. Palleschi, Phys. Rev. A **30**, 3241 (1984).
[3] D. Yelin, Y. Silberberga, Y. Barad, and J. S. Patel, Appl. Phys. Lett. **74**, 3107 (1999).
[4] B. Jérôme, Rep. Prog. Phys. **54**, 391 (1991).
[5] H. Yokoyama, S. Kobayashi, and H. Kamei, Mol. Cryst. Liq. Cryst. **129**, 109 (1985).
[6] D. Todorović-Marinić and J. T. Gleeson, Phys. Rev. E **54**, 5227 (1996).
[7] T. J. Sluckin and A. Poniewierski, in *Fluid Interfacial Phenomena*, edited by C. A. Croxton (Wiley, New York, 1986).
[8] A. Poniewierski, Liq. Cryst. **24**, 1369 (2000).
[9] G. D. Wall and D. J. Cleaver, Phys. Rev. E **56**, 4306 (1997).
[10] G. D. Wall and D. J. Cleaver, Mol. Phys. **101**, 1105 (2003).
[11] D. J. Cleaver and M. P. Allen, Mol. Phys. **80**, 253 (1993).
[12] M. Dijkstra, R. van Roij, and R. Evans, Phys. Rev. E **63**, 051703 (2001).
[13] T. J. Sluckin and A. Poniewierski, Phys. Rev. Lett. **55**, 2907 (1985).
[14] I. Lelidis, Liq. Cryst. **25**, 531 (1998).
[15] R. James, F. A. Fernández, S. E. Day, M. Komarcevic, and W. A. Crossland, Mol. Cryst. Liq. Cryst. **422**, 479 (2004).
[16] G. Derfel, Liq. Cryst. **27**, 829 (1998).
[17] M. P. Lettinga and J. K. G. Dhont, J. Phys.: Condens. Matter **16**, S3929 (2004).
[18] P. D. Olmsted and C. Y. David Lu, Phys. Rev. E **60**, 4397 (1999).
[19] P. Sheng and E. B. Priestley, in *Introduction to Liquid Crystals*, edited by E. B. Priestley, P. J. Wojtowicz, and P. Sheng (Plenum, New York, 1975).
[20] V. Popa-nita and T. J. Sluckin, J. Phys. II **6**, 873 (1996).
[21] A. Šarlah and S. Žumer, Phys. Rev. E **60**, 1821 (1999).
[22] B. Zappone, Ph. Richetti, R. Barberi, R. Bartolino, and H. T. Nguyen, Phys. Rev. E **71**, 041703 (2005).
[23] D. J. Cleaver and P. I. C. Teixeira, Chem. Phys. Lett. **338**, 1 (2001).